Check for updates

Discrimination Between Small Earthquakes and Quarry Blasts in Egypt Using Spectral Source Characteristics

I. M. Korrat,[1] Ahmed Lethy,[2] (iD) M. N. ElGabry,[2] (iD) H. M. Hussein,[2] (iD) and Adel S. Othman[2] (iD)

Abstract—Source parameters calculated from displacement spectra of both P and S waves are used to discriminate between earthquakes and quarry blasts in three regions of Egypt during the 2009–2015 period. We use vertical component seismograms from 440 earthquakes and 450 quarry explosions with M_D 1.5 to 3.3 to calculate source parameters, including scalar moments and corner frequencies. The $M_o(P,S)$ vs. $f_c(P,S)$ and P- to S-wave corner frequency $f_c(P)/f_c(S)$ ratios are used to distinguish quarry blasts from earthquakes. A comparison of $M_o(P,S)$ vs. $f_c(P,S)$ for both earthquakes and explosions in Egypt demonstrates that explosions had significantly lower corner frequencies than earthquakes, particularly for S-wave displacement spectra. In contrast to the Northern and Central regions, the Southern Egyptian region provides a perfect separation of corner frequencies of earthquakes and explosions for both P- and S-waves. The empirically derived average ratio of $f_c(P)/f_c(S)$ for earthquakes is 1.28, 1.26 and 1.26 in the Northern, Central and Southern Egyptian regions, respectively. For explosions, average $f_c(P)/f_c(S)$ ratios are 1.89, 1.86 and 2.0 in the three Egyptian regions, respectively. According to these findings, the average ratio of $f_c(P)$ to $f_c(S)$ for explosions is higher than those for earthquakes, implying that the differences in ratios enhance the ability of the $f_c(P)$ vs. $f_c(S)$ approach to discriminate between earthquakes and explosions. Based on the average $f_c(P)/f_c(S)$ ratios vs. M_w in the whole of Egypt, the observed $f_c(P)/f_c(S)$ discrimination threshold value for separating quarry explosions from earthquakes is 1.51–1.52.

Keywords: Seismic discrimination, Spectral analysis, Source parameters, Corner frequency, Earthquakes, Explosions.

[1] Geology Department, Faculty of Science, Mansoura University, Mansoura, Egypt.
[2] National Research Institute of Astronomy and Geophysics (NRIAG), Helwan, Cairo 11421, Egypt. E-mail: alethy@nriag.sci.eg

1. Introduction

The Egyptian National Seismological Network (ENSN), which is spread across the country, plays a key role in monitoring seismic events, both natural earthquakes and artificial explosions. Several quarries in Egypt use blasting to handle the mobility of rock masses. Trustable discrimination of human-made explosions is presently becoming a significant issue in seismic observations by both local and regional seismic networks. Distinguishing between small-magnitude events remains a challenging task.

Among the techniques used for discrimination are ratios of amplitudes of various seismic phases (e.g., Anderson et al., 2009; McLaughlin et al., 2004) and velocity spectra assessment (e.g., Gitterman et al., 1998; Walter et al., 1995). Other investigation methods include spectral recognition of certain wave groups, spectral ratios of the seismic phases and spectrograms (e.g., Allmann et al., 2008; Dahy & Hassib, 2010; Hammer et al., 2013; Koch & Fäh, 2002). A significant number of studies have used short-period records for discrimination in specific regions (e.g., Horasan et al., 2009; Yilmaz et al., 2013). Yavuz et al. (2019) performed the discrimination between earthquakes and explosions that occurred in the Armutlu Peninsula area, northwestern Turkey, using the power spectrum density (PSD) discrimination method. They noted that the power spectra of quarry blasts decreased more sharply with increasing frequencies than those of earthquakes. Sertçelik al. (2020) conducted a study in the Eastern Marmara region, Turkey, using the amplitude peak ratio, complexity, spectral ratio and continuous wavelet transform (CWT) discrimination methods. They found that 182 of the recorded seismic events

were caused by artificial explosions, while 395 events were classified as earthquakes.

Displacement spectra of the P- and S-waves recorded by short-period stations for both local earthquakes and quarry blasts of comparable magnitudes in Israel and Lebanon have been inspected and evaluated by Ataeva et al. (2017). According to their findings, the calculated ratios of P- to S-wave corner frequency $f_c(P)/f_c(S)$ computed for each event have demonstrated significant segregation between earthquake and quarry blast groups. Explosions also have lower corner frequencies (f_c) than earthquakes, particularly for S-wave displacement spectra, as shown by the M_o vs. f_c relationship for earthquakes and explosions.

This study applies the spectral analysis technique for discrimination between earthquakes and quarry blasts (explosions). Following the approach of Ataeva et al. (2017), the average values of the corner frequency ratio $f_c(P)/f_c(S)$ and M_o vs. f_c of multiple displacement spectra stations for both earthquakes and quarry explosions in three Egyptian regions (Northern, Central and Southern) are investigated to establish statistical discrimination criteria for segregation. Each region is checked individually to identify variations that can distinguish any of them. We also investigate the relationship between the $f_c(P)/f_c(S)$ ratio and the moment magnitude M_w of both P- and S-waves for the whole of Egypt.

2. Data Source

The waveform data used in this study consist of 3416 vertical component seismograms from 440 earthquakes and 450 quarry explosions with M_D 1.5–3.3, which occurred at epicentral distances up to 200 km during the 2009–2015 periods. The broadband and short-period stations data of ENSN are extracted from the database. Earthquakes of depths < 25 km were used. Most quarry blasts are identified from monthly reports of quarries received by the ENSN main center independently of seismic means. In this study, we rely on solutions under the condition that the seismic event was recorded by at least three seismic stations located at different epicentral distances with a reasonable signal-to-noise ratio

(SNR $\geq$ 10). We used the software code offered by Kumar et al. (2014) to determine the SNR of P- and S-waves. SNR is calculated by dividing the Fourier amplitude spectrum estimated from a P or S window of the signal by the Fourier amplitude spectrum calculated from a noisy window of the same duration, which is frequently selected before the event. The data processing software EQK_SRC_PARA (Kumar et al., 2012) was used in the analysis. The hypocentral parameters and duration magnitudes of the studied events were determined using ATLAS program, provided by Nanometrics Inc., Canada, for seismic data analysis using the 1D velocity-depth model of EI-Hadidy (1995).

ENSN stations involve different seismometers: short period SS-1 Ranger with 1-Hz natural frequency, L4C type, broadband 120 s Streckeisen STS-2 seismometers, Trillium 40 and Trillium 120 s (Fig. 1). The sampling rate of the recorded data is 100 samples per second. According to the distribution of both earthquakes and quarry explosions, Egypt is divided into three main regions (Fig. 2): Northern (including subzones 1, 2 and 3); Central (including subzones 4 and 5) and Southern Egypt (including subzone 6). For reliable and robust discrimination analysis, comparable magnitudes and close spatial distribution for earthquakes and explosions are maintained (Figs. 2, 3). Figures 4, 5 demonstrate a time-domain comparison between earthquake and explosion, using waveforms for two events having similar magnitudes and were recorded by the same stations and located almost at the same epicentral distances. It is evident that the displayed waveforms reveal the difference between an earthquake and an explosion, clarifying the quality of S-waves produced by explosions. In some cases, S-waves for quarry blasts are poorly created and S-wave windows could be possibly contaminated by long period surface waves (Rg-type energy) (Fig. 4) or dominated by clear first arrival compressional P-wave (Fig. 5), thus indicating the character of blasting. Additional waveforms from different zones are available in the supplementary materials.
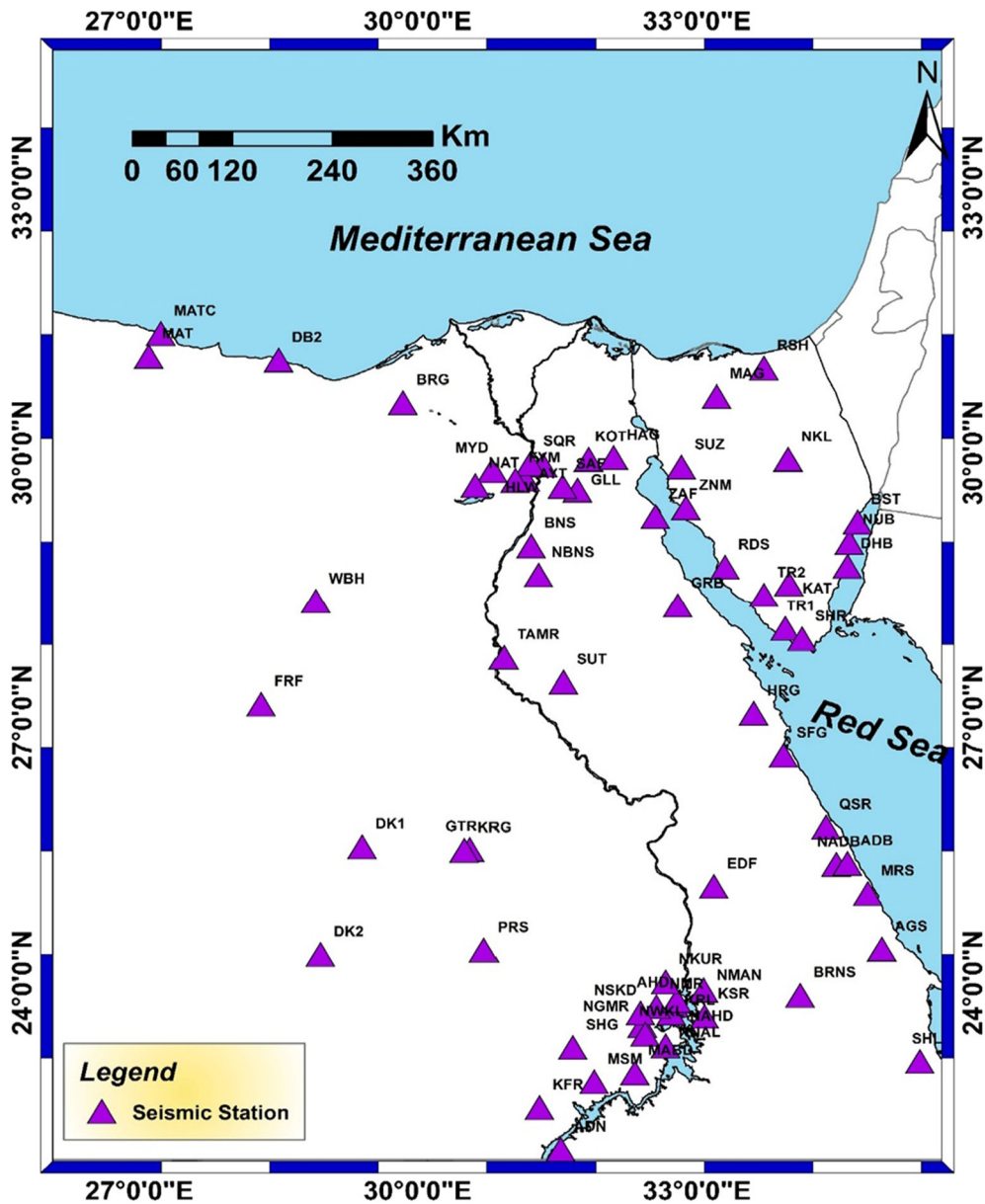
Figure 1
Geographical distribution of the Egyptian National Seismological Network (ENSN)

3. Spectral Analysis

3.1. Data Processing

Spectral analysis is one of the most valuable screening methods to differentiate between earthquakes and explosions. The source parameters for all events were investigated using the P- and S-wave displacement amplitude spectra obtained from the vertical component seismograms according to the omega-square source model of Brune (1970, 1971), considering attenuation effects to geometrical spreading and anelastic attenuation. The main reason for using the vertical component is that most ENSN stations during the study period have a single vertical component. Moreover, the vertical component averts
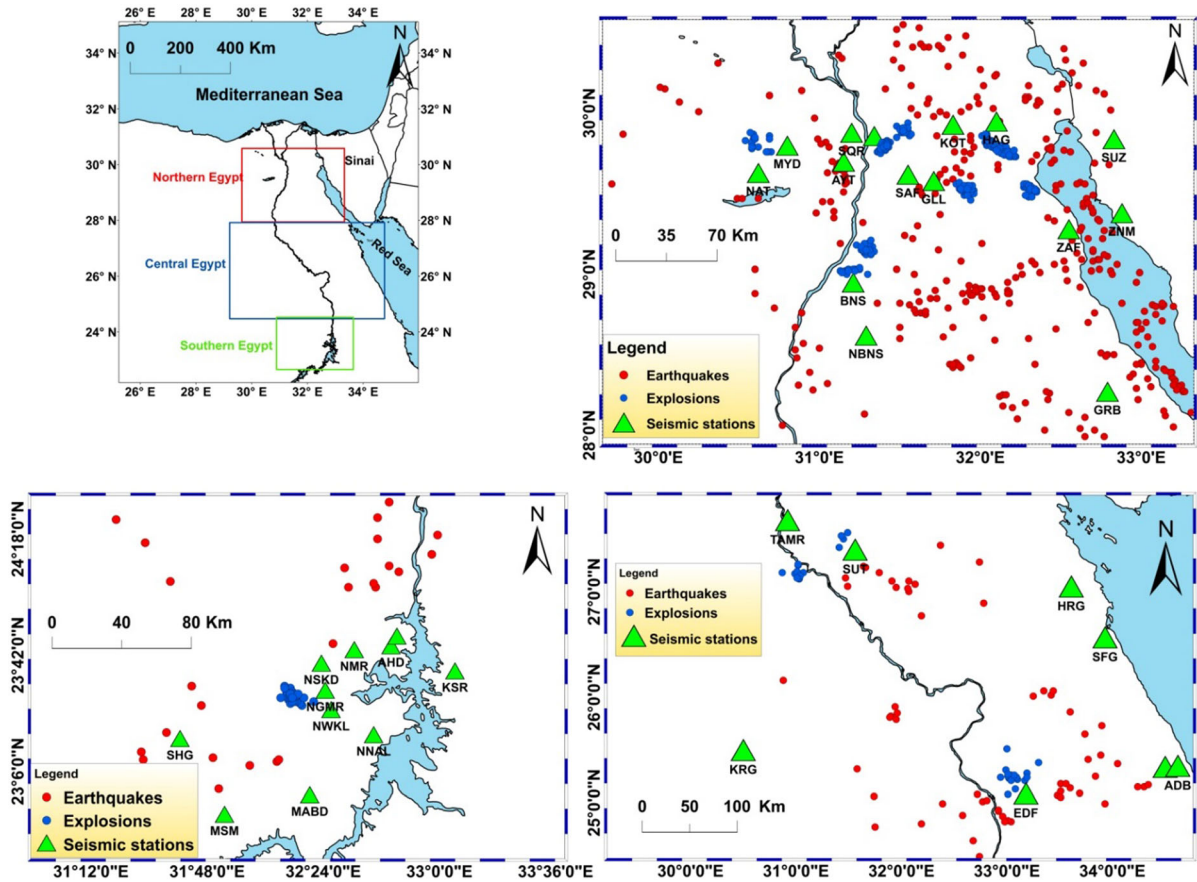
Figure 2
Location map of earthquakes (red) and explosions (blue) recorded by ENSN seismic stations (green triangles) in the three main regions in Egypt; Northern, Central and Southern zones
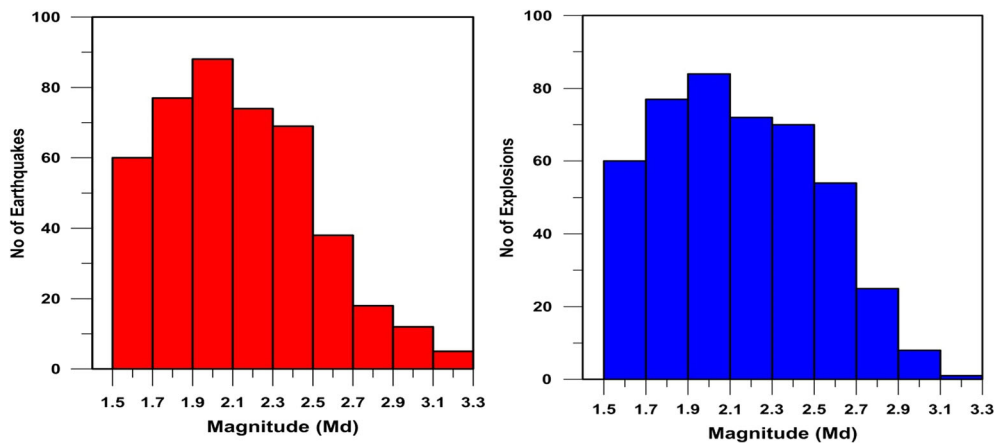

Figure 3
Histograms of duration magnitudes: of earthquakes, red (left panel) and explosions, blue (right panel) used in the study
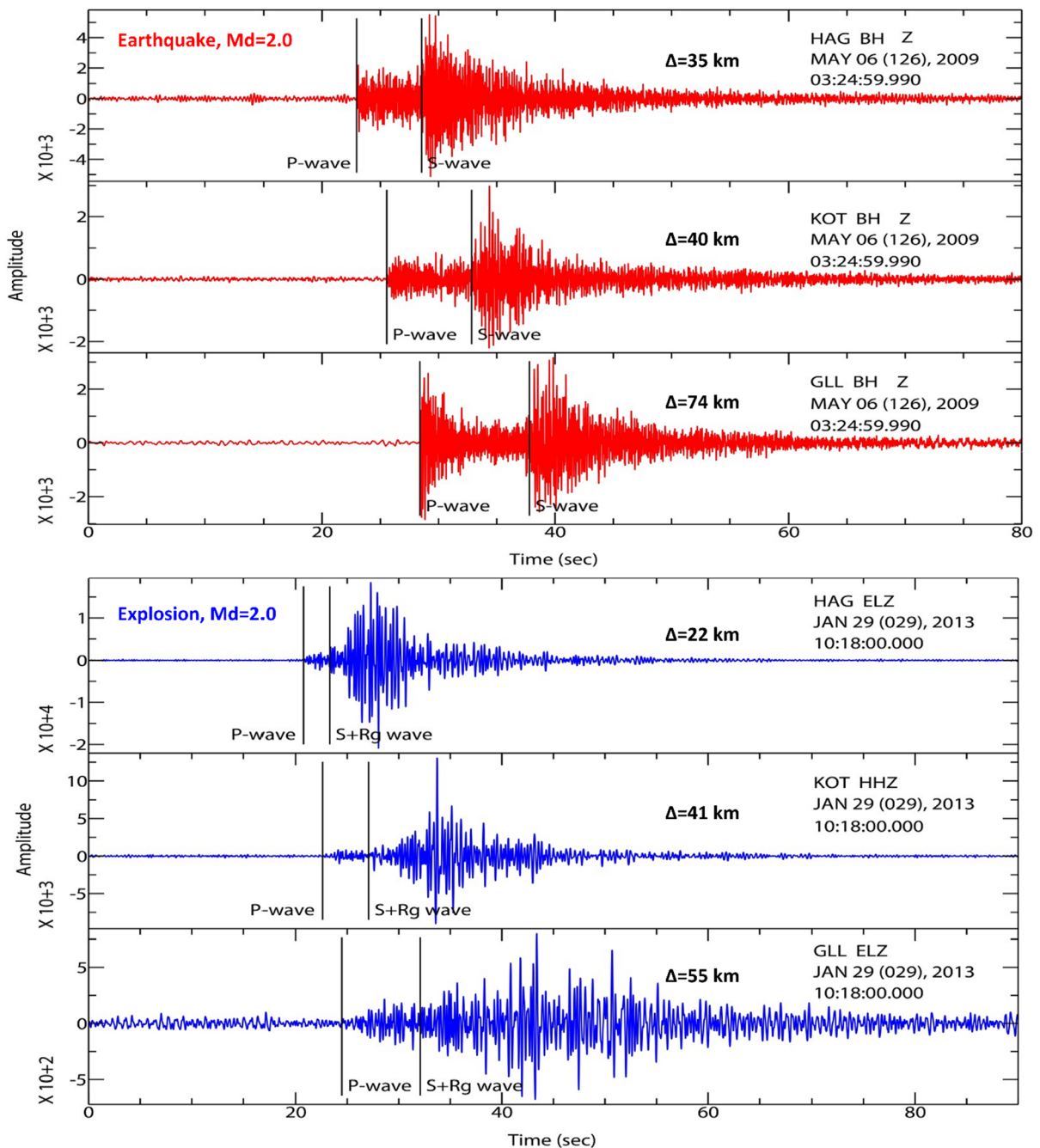
Figure 4
Original vertical component seismograms before data processing of an earthquake on 6 May 2009, $M_d = 2.0$ (red) and of a quarry blast on 29.01.2013, $M_d = 2.0$ (blue) in subzone 1, Northern region. The arrivals of P-wave, S-wave and epicentral distance values Δ of recorded stations (HAG, KOT and GLL) are also shown

any site effects or spectral complexity. EQK_SRC_-PARA software of Kumar et al. (2012) was used to calculate the displacement amplitude spectra. The first step in the signal pre-processing is to remove the
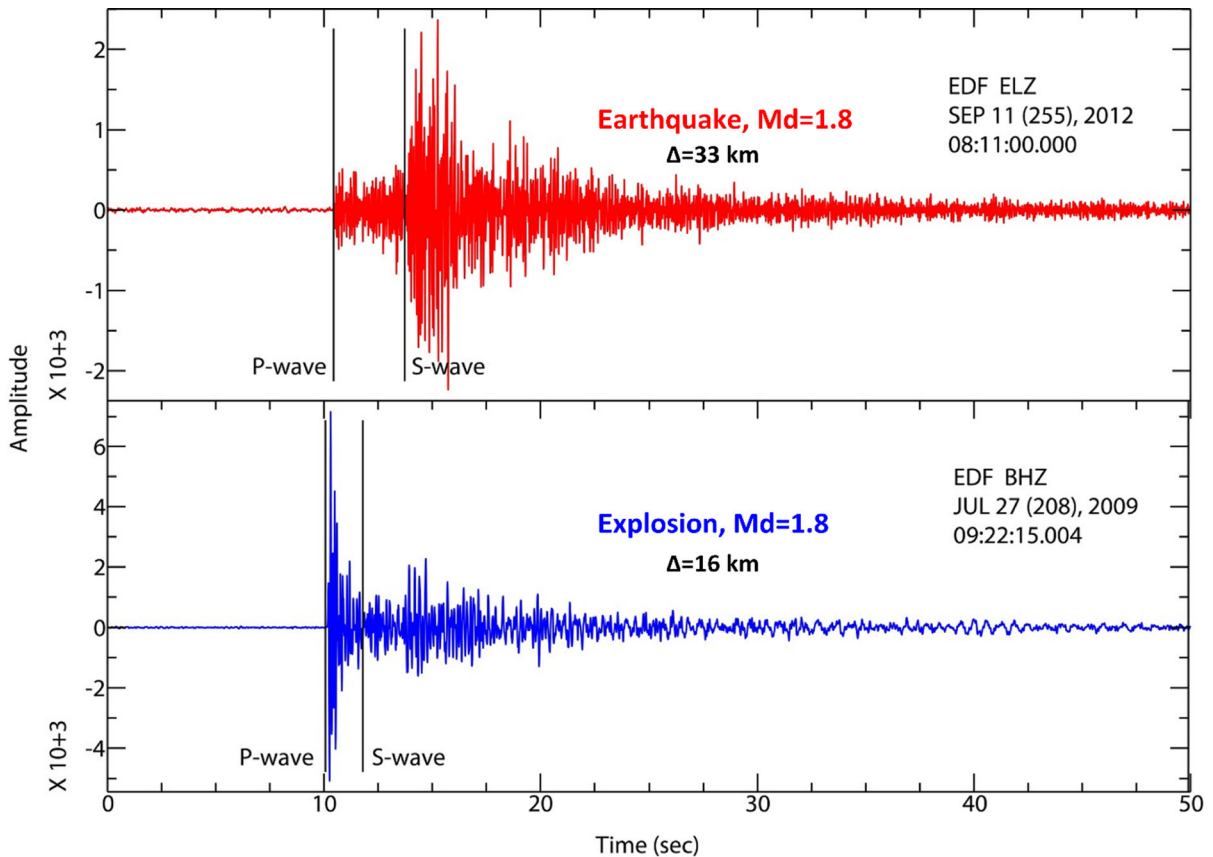
Figure 5

Original vertical component seismograms before data processing of an earthquake on 11 September 2012, M_d = 1.8 (red) and of a quarry blast on 27 July 2009, M_d = 1.8 (blue) in subzone 5, Central region. The arrivals of P-wave, S-wave and epicentral distance values Δ of recorded EDF station are also shown

mean and linear trends. The second step is to perform deconvolution to remove the instrumental effect from each station seismogram, using a designed filter with the coefficient of poles, zeros and combined sensitivity of both sensor and digitizer. Once the signal was corrected, the seismograms were transformed from counts to m/s.

Consequently, we manually picked the appropriate range of P- and S-wave time windows in seconds for each seismogram, always starting at the first arrival times of P- and S-waves, which were picked manually on the vertical component seismogram. Several checks with different durations of P- and S-waves were performed to select the optimum signal window length that would avoid interference from other phases and ensure the resolution and

stabilization of amplitude spectra. The selected P-wave window length covers the first P-phase group; it ranges from 1.5 to 4 s. The S-wave's selected time window usually ranges from 10 to 20 s, depending on distances. This window includes the most significant part of the signal energy, as generally accepted for estimating the seismic moment (Baumbach & Borman, 2012; Brune, 1970, 1971; Hanks & Wyss, 1972). At short distances, most quarry blast S-wave time windows also include the surface Rg phase (actually very weak S-wave + Rg-wave windows) (Fig. 3). The amplitude Rg wave is strongly depth-dependent; it is often observed in near-surface events such as quarry blasts with large amplitudes (e.g., McLaughlin et al., 2004) and not usually observed in earthquakes with depths greater than a
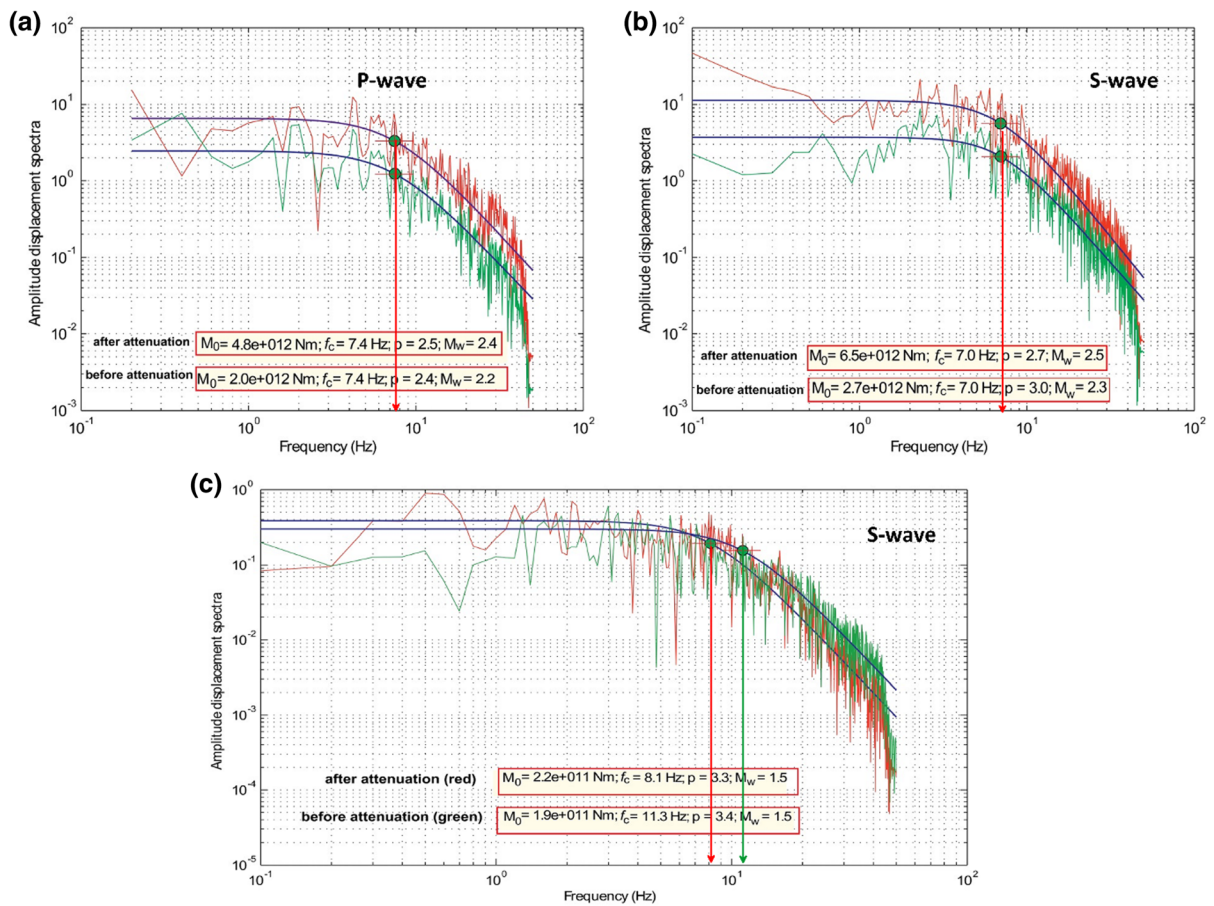
Figure 6

Observed P-wave (**a**) and S-wave (**b**) displacement spectra of an earthquake (28 October 2012, M_d = 2.5) before (green) and after (red) correction for attenuation effects together with the best-fitting theoretical Brune's spectra (blue). This is calculated from seismograms of the HAG station located 50 km from the earthquake epicenter. **c** Observed S-wave displacement spectra of an earthquake (31 January 2012, M_d = 1.6) before (green) and after (red) correction for attenuation effects together with the best-fitting theoretical Brune's spectra (blue). This is calculated from seismograms of the HAG station located 26 km from the earthquake epicenter. Also, the measured M_o, f_c, absolute value of spectral decay slope at high frequencies (P) and moment magnitude M_w are marked. The value of corner frequency is marked by red and green lines

few km. Based on the work of Ataeva et al. (2017), the long S-wave window offers the optimum results for discrimination between earthquakes and explosions. After selecting the windows, integration must be done to obtain the displacement waveforms using the cumulative trapezoidal numerical integration technique. To obtain the displacement spectra of the specific time window of P- and S-waves for each vertical velocity record, the fast Fourier transform (FFT) is carried out.

The obtained displacement spectrum was corrected for both geometric spreading and anelastic attenuation. If the attenuation correction was not neglected, two effects were produced; the spectrum form changes, which affects the corner frequency assessment and influences the low-frequency level, which consequently affects the seismic moment calculation. Therefore, the correction for attenuation is particularly important to obtain a reliable corner frequency. It also contributes to correcting the flat part of the spectrum in the case of small earthquakes with high-frequency content (Süle & Wébe, 2013). In this study, based on the equation $G(R) = 1/R$, geometrical spreading is assessed for body waves
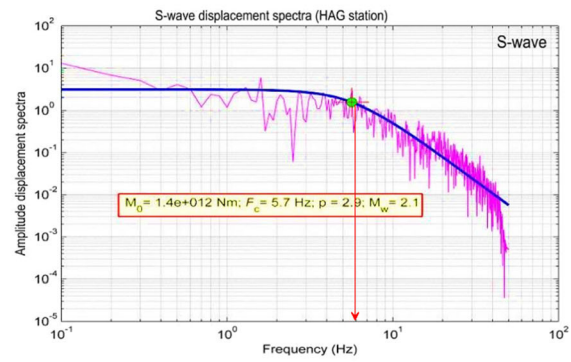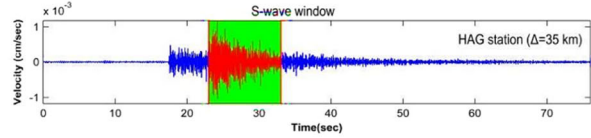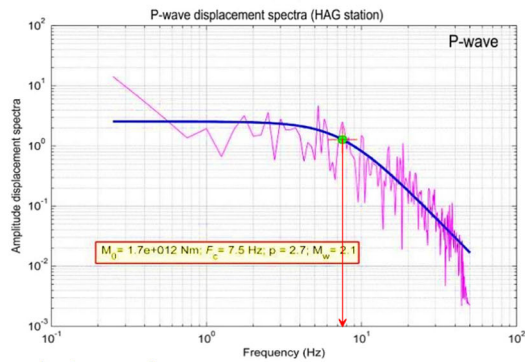
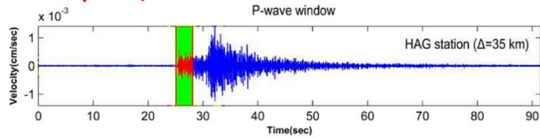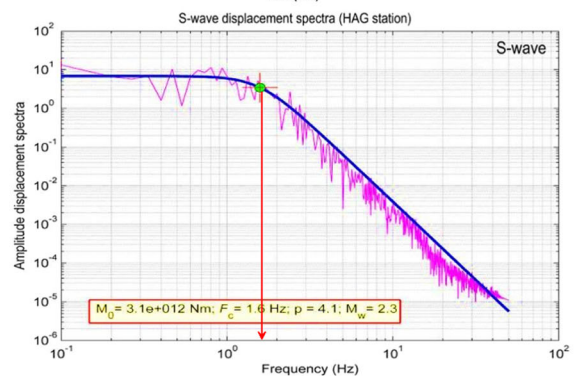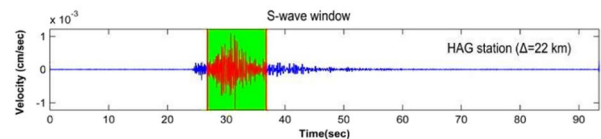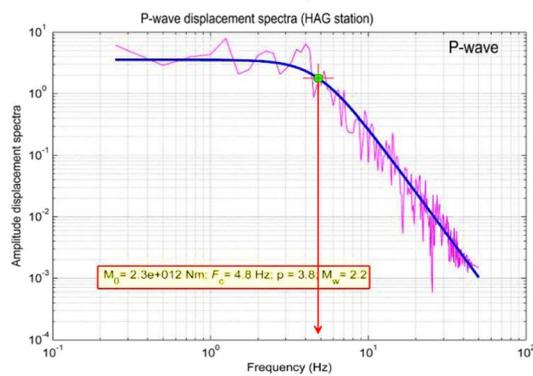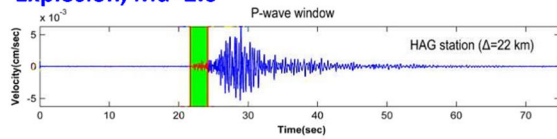Figure 7

Original vertical component seismograms before data processing of an earthquake on 6 May 2009, M_d = 2.0, and of a quarry blast on 29 January 2013, M_d = 2.0, in subzone 1, Northern region. The arrivals of P-wave, S-wave and epicentral distance values Δ of the recorded station (HAG) are also shown. The corrected P- and S-wave displacement spectra after data processing were calculated from seismograms of the HAG station located 35 km from the earthquake and 22 km from the quarry blast epicenter. The analyzed time windows of P- and S-waves are marked by highlighted green rectangles. The best-fitting theoretical Brune's source model is marked in blue. Also, the measured M_o, f_c, absolute value of spectral decay slope at high frequencies (P) and moment magnitude M_w are shown. The red line shows the value of the corner frequency f_c

(Havskov & Ottemöller, 2010). This research focuses on short distances; S-waves can be handled as P-waves. Correction of the anelastic attenuation that includes attenuation due to path effect $\exp[-\pi f t / Q(f)]$, with the frequency-dependent quality factors (Q_P and Q_S) of P- and S-waves and the attenuation near the site $\exp[-\pi f \kappa]$, with (κ) parameters (Singh et al., 1982), was performed. The following relations—$Q_S(f) = 85.66 \ f^{0.79}$ (El-Hadidy et al., 2006), $Q_S(f) = 56 \ f^{1.1}$ (Morsy et al., 2013) and $Q_S(f) = 54 \ f^{1.16}$ (Mukhopadhyay et al., 2016)—are available for the estimation of the frequency-dependent S-wave quality factors in Northern, Central and Southern Egypt, respectively. For $Q_P(f)$, there are no available
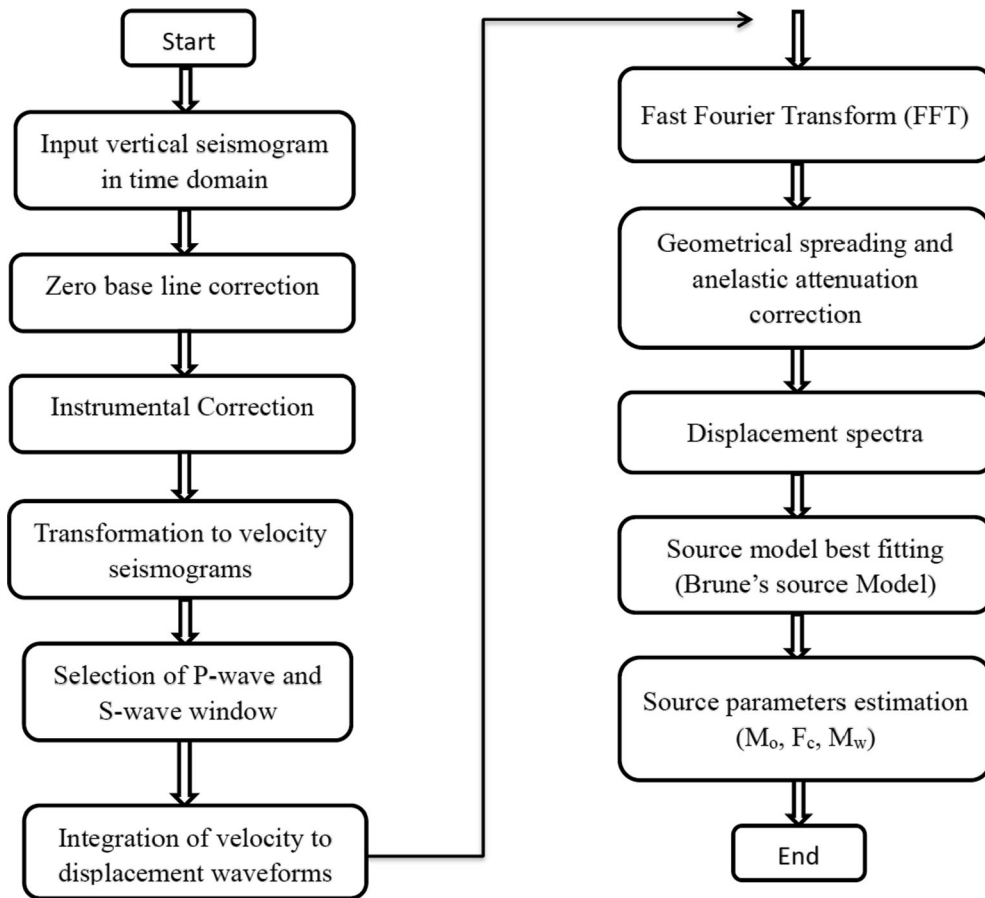
Figure 8
Flowchart of procedure adopted in EQK_SRC_PARA software for estimation of displacement spectra and source parameters for studied events

Table 1

Velocity model of El-Hadidy (1995)

P-wave velocity (km/s)	S-wave velocity (km/s)	Depth (km)	ρ (g/cm^3)
4.5	2.57	0.0	2.6
6.0	3.42	3.5	2.8
6.5	3.71	16.0	3.0
8.0	4.57	31.0	3.2

V_S is calculated using $V_P/V_S = 1.75$

relationships for Egypt. Therefore, the findings of Abercrombie and Leary (1993) will be considered with $Q_P = 2Q_S$ near the surface. Anderson et al. (1965) obtained similar results in a study of Q in the upper mantle where $Q_P = 2.25\ Q_S$. Furthermore,

Barton (2007) calculated Q_P independently from the empirical equation $Q_P = (V_P/V_S) \cdot Q_S$. Adopting the above results, we assume the relation $Q_P(f) = 2QS(f)$ for the frequency-dependent P-wave quality factor in this study. In Egypt, the kappa (κ) factor estimated by previous studies varied from 0.01 to 0.03 s (Abou Elenean et al., 2010). For the small earthquakes with very high-frequency content, the near surface correction (κ) enabled recognizing the masked corner frequencies in the high-frequency spectral decay.

Figure 6 illustrates the effect of attenuation correction on displacement spectra together with the theoretical Brune's model. Because the exponent of the frequency f in $Q(f)$ relations used in this study is close to unity, the path-dependent attenuation

depends slightly on frequency. In this case, the Q correction practically has a slight change in the shape of the P- and S-wave spectra. It affects only the low-frequency spectral level, affecting the scalar moment (M_o and M_w) estimation. On the other hand, the attenuation correction for the small earthquakes with significant high-frequency content causes slight changes in the low spectral level. This affects the spectrum's shape, causing a shift in the corner frequency f_c. Moreover, the near-surface attenuation correction is also essential for obtaining the true values of corner frequency f_c for small earthquakes.

Once the corrected displacement spectra were obtained, the nonlinear least-square inversion technique was performed to fit Brune's source model using EQK_SRC_PARA software to estimate the spectral parameters, including the low-frequency spectral amplitude (Ω_0) and the corner frequency (f_c) at the source according to Eq. (1). Consequently, EQK_SRC_PARA software automatically calculates the source parameters for both studied earthquakes and explosions, including scalar moments (M_o and M_w) based on the Eqs. (2) and (3). The fitted theoretical Brune's curve of the computed displacement spectra is defined by two lines, which refer to the low-frequency spectral plateau and high-frequency decay of f^{-2}. The calculated corner frequency is a boundary point in the frequency response at which spectral energy flowing through the signal begins to be reduced (attenuated) rather than passing through (at which the spectrum begins to decay at a higher frequency). It is also defined as the intersection point of the low- and high-frequency asymptotes (e.g., Baumbach & Borman, 2012; Brune, 1970; Havskov & Ottemöller, 2010; Kiratzi &

Louvari, 2001; Motlagh & Mostafazadeh, 2008). Figure 7 shows an example of the corrected displacement spectra of an earthquake and an explosion in the Northern region. Additional examples are available in the supplementary materials.

A flow chart of the procedure used to estimate the displacement spectra and source parameters for the studied events is given in Fig. 8.

$$D(f) = \frac{\Omega_0}{\left(1 + \frac{f}{f_c}\right)^s} = \frac{M_o \cdot \Re\theta\varphi \cdot F \cdot G\left(\Delta, h\right)}{\left(1 + \frac{f}{f_c}\right)^s 4\pi\rho v^3}. \quad (1)$$

The seismic moments (M_o(P) and M_o(S)) of the investigated earthquakes and explosions for each event-station pair are estimated (Eq. 2) according to Brune's source model for both P- and S-waves separately (Brune, 1970; Hanks & Wyss, 1972):

$$M_o = \frac{4\pi\rho V^3 \Omega_o R}{F * \Re\theta\varphi}, \quad (2)$$

where V is the velocity (V_P or V_S) extracted from Table 1, according to the source depth, Ω_0 is the low-frequency spectral level, R is the epicentral distance, ρ is the density, $\Re\theta\varphi$ is the radiation pattern, and F is the free surface effect (assumed to be 2) calculated for the individual stations based on V_P/V_S and the emergence angles of P- and S-waves using the free surf program of Snoke (2003). The average values of radiation pattern coefficient $\Re_p(\theta, \varphi) = 0.64$ (Baumbach & Borman, 2012) for P-waves and $\Re_s(\theta, \varphi) = 0.55$ for S-waves (Boore & Boatwright, 1984) are used in this study. According to the concept of Hanks and Kanamori (1979), the moment magnitude M_w of the examined earthquakes and explosions

Table 2

Estimated standard deviation value σ in logarithmic units of source parameters (f_c, M_o and M_w) for all earthquakes and explosions in Egypt for P- and S-wave spectra, separately

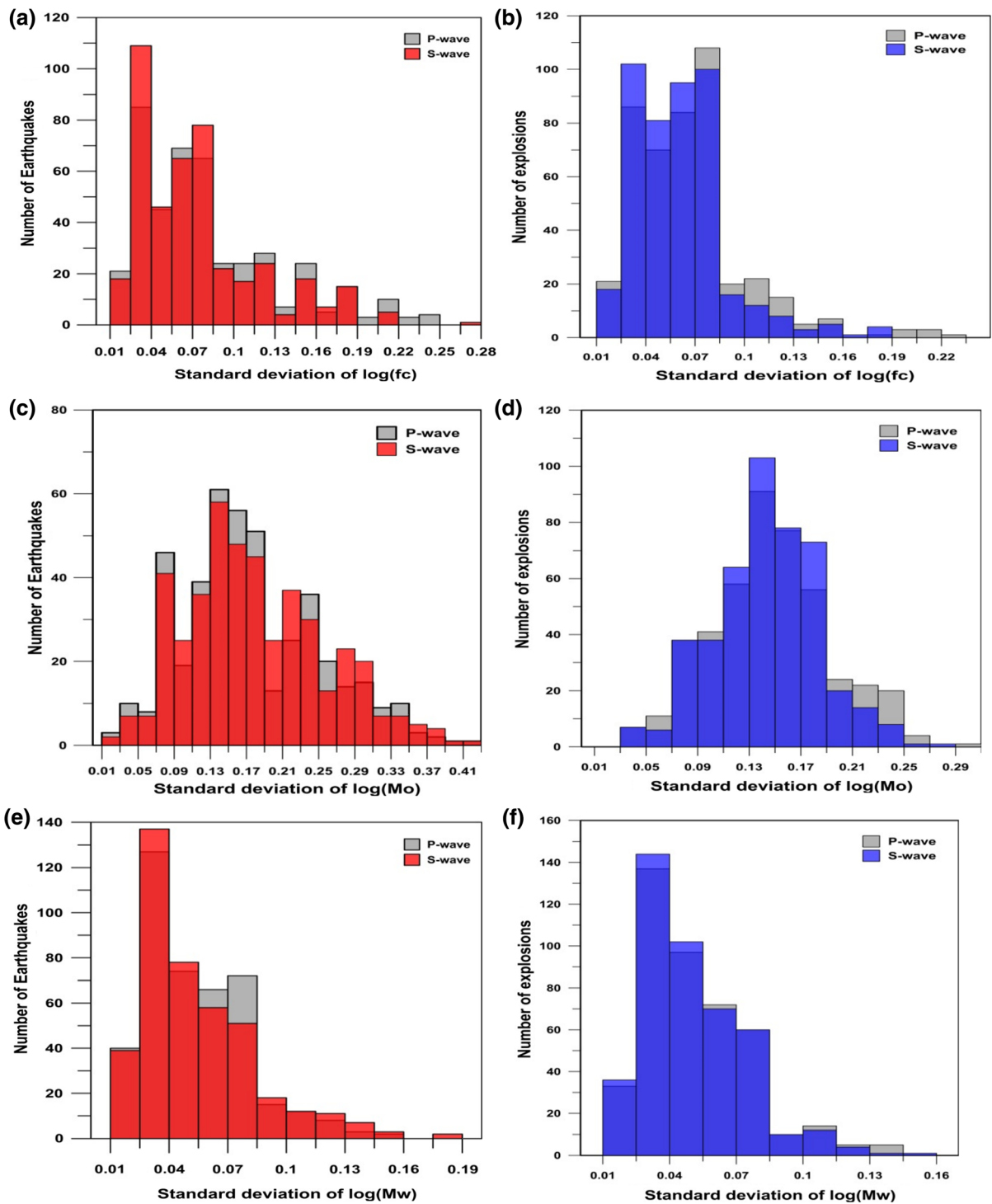| Events	f_c standard deviations		M_o standard deviations		M_w standard deviations	
	P-wave	S-wave	P-wave	S-wave	P-wav	S-wav
Earthquakes	0.01–0.24 σ_{avg} (0.066)	0.01–0.27 σ_{avg} (0.060)	0.02–0.42 σ_{avg} (0.16)	0.01–0.40 σ_{avg} (0.17)	0.01–0.15 σ_{avg} (0.045)	0.01–0.19 σ_{avg} (0.044)
Explosions	0.01–0.23 σ_{avg} (0.059)	0.01–0.19 σ_{avg} (0.055)	0.04–0.30 σ_{avg} (0.14)	0.04–0.28 σ_{avg} (0.14)	0.01–0.15 σ_{avg} (0.046)	0.01–0.15 σ_{avg} (0.045)

Figure 9
Histograms of the standard deviations for the logarithmic corner frequency (**a**, **b**), logarithmic seismic moment (**c**, **d**) and logarithmic moment magnitude (**e**, **f**) for all studied earthquakes (red) and explosions (blue), respectively in Egypt
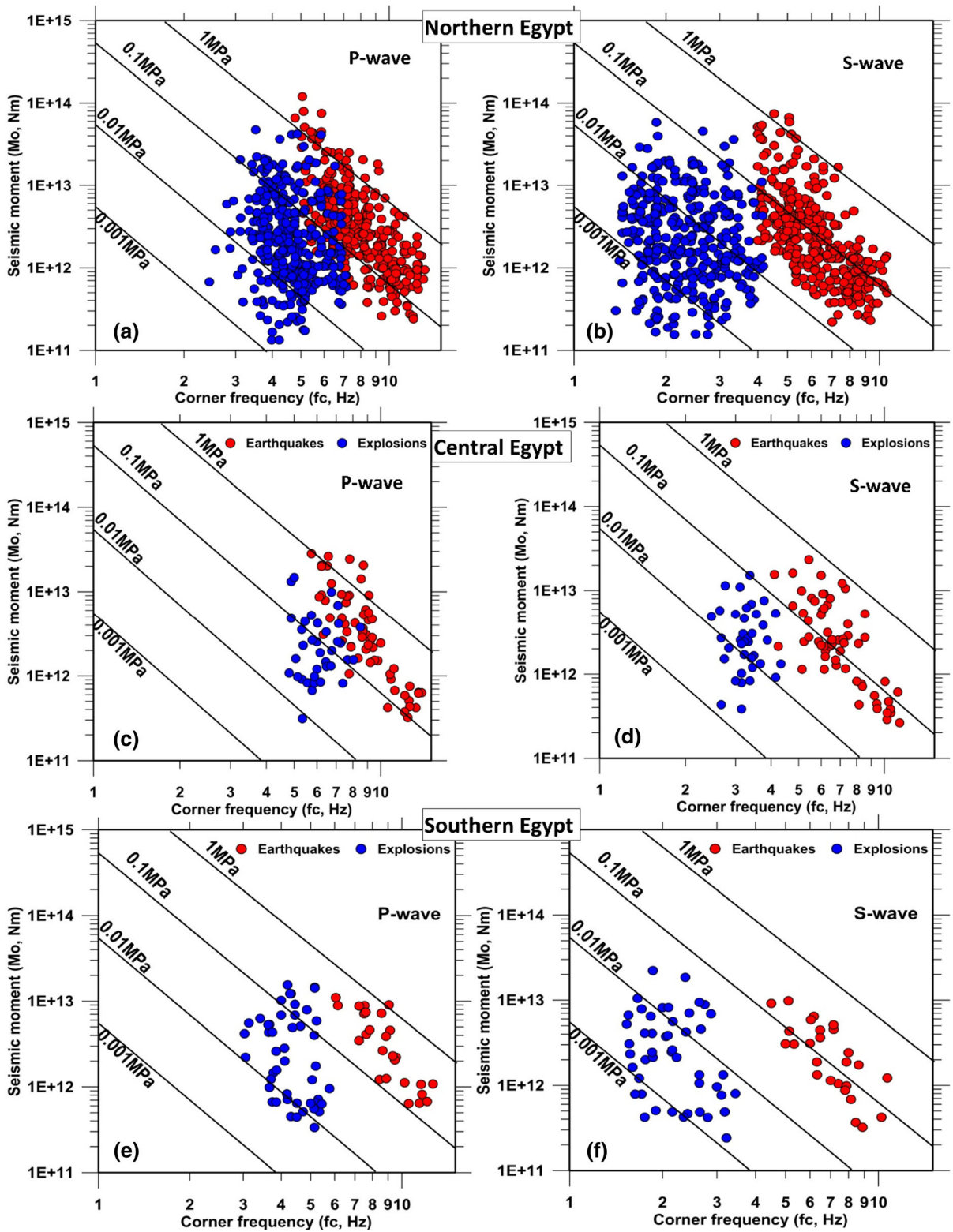
◀Figure 10
Seismic moment M_o vs. corner frequency f_c for studied earthquakes (red) and explosions (blue) in Northern, Central and Southern Egypt obtained from P-waves (**a**, **c**, **e**) and S-waves (**b**, **d**, **f**). The black solid lines indicate the constant stress drop in accordance with Brune's source model

at the source is calculated using the following equation:

$$M_w = \frac{2}{3} \log(M_0) - 10.73. \qquad (3)$$

The average value for corner frequencies f_c, seismic moments M_o and moment magnitudes M_w for each event, and their standard deviation, is estimated from the spectra for P- and S-waves recorded by different stations (i). Thus, a more accurate evaluation of these parameters is obtained. Averaging the source parameters reduces the scattering induced by different station azimuths, particularly for P-waves. Following the equations suggested by Archuleta et al. (1982), average parameters are estimated for both P- and S-waves separately:

$$x_{avg} = \text{antilog} \left(\frac{1}{N} \sum_{i=1}^{N} \log x_i \right) \qquad (4)$$

$$\text{SD}\left[\log x_{avg}\right] = \left[\frac{1}{N-1} \sum_{i=1}^{N} \left(\log x_i - \log x_{avg}\right)^2 \right]^{1/2}, \qquad (5)$$

where x points to f_c (P, S) or M_o (P, S) or M_w (P, S), and x_{avg} indicates the average value of x. N is the number of the stations used; $\text{SD}\left[\log x_{avg}\right]$ represents the standard deviation of the logarithm.

3.2. Discrimination Analysis Using Source Parameters

3.2.1 Seismic Moment Vs. Corner Frequency

The average f_c, M_o and M_w values estimated from the multiple available stations for every earthquake and explosion are used in the comparative discrimination analysis for P- and S-waves separately. The standard deviations of source parameters (f_c, M_o and M_w) are estimated for each event to obtain a reliable discrimination analysis. The maximum number of stations used in these estimations is 8 and 6 for each earthquake and explosion, respectively. Table 2 shows the calculated values of standard deviations of the estimated corner frequencies f_c, seismic moment M_o and moment magnitudes M_w from P- and S-waves separately in logarithmic units for all studied earthquakes and explosions in Egypt. The average standard deviations values σ of corner frequency estimations were acceptable and practically validated for both earthquakes and explosions, as required for the comparative discrimination analysis confidence (Fig. 9).

For both earthquakes and explosions in Northern, Central and Southern Egypt, seismic moments M_o vs. corner frequencies f_c were compared individually for P- and S-waves (Fig. 10). This figure demonstrates that the seismic moments M_o of earthquakes and explosions are almost located within the same range. The corner frequencies of the S-wave displacement spectra show a better separation between earthquakes and explosions than those of the P-wave spectra. The relation between f_c and M_o also shows a more significant separation between earthquakes and explosions for P- and S-waves in Southern Egypt than in Northern and Central Egypt regions. Comparing the corner frequencies of earthquakes and explosions in Northern, Central and Southern Egypt for P- and S-waves indicates that explosions show markedly lower corner frequencies f_c than earthquakes, particularly for S-wave displacement spectra (Fig. 11). This figure displays a minor overlap in the corner frequencies of earthquakes and explosions for both Northern and Central Egypt. In Northern Egypt, this overlap is smaller for S-waves (1.25%) than for P-waves (11.7%), while Central Egypt shows an overlap of 18% and 0.06% for P- and S-waves, respectively.

In contrast, the Southern Egypt region observed a strong complete distinction between corner frequency values of earthquakes and explosions. In all Egyptian zones for earthquakes, the corner frequency values f_c(P) and f_c(S) manifest wide frequency ranges while explosions display narrow frequency bands. The shift of f_c(P) relative to f_c(S) is smaller for earthquakes than for explosions in Egypt. Table 3 demonstrates the estimated corner frequency values for earthquakes
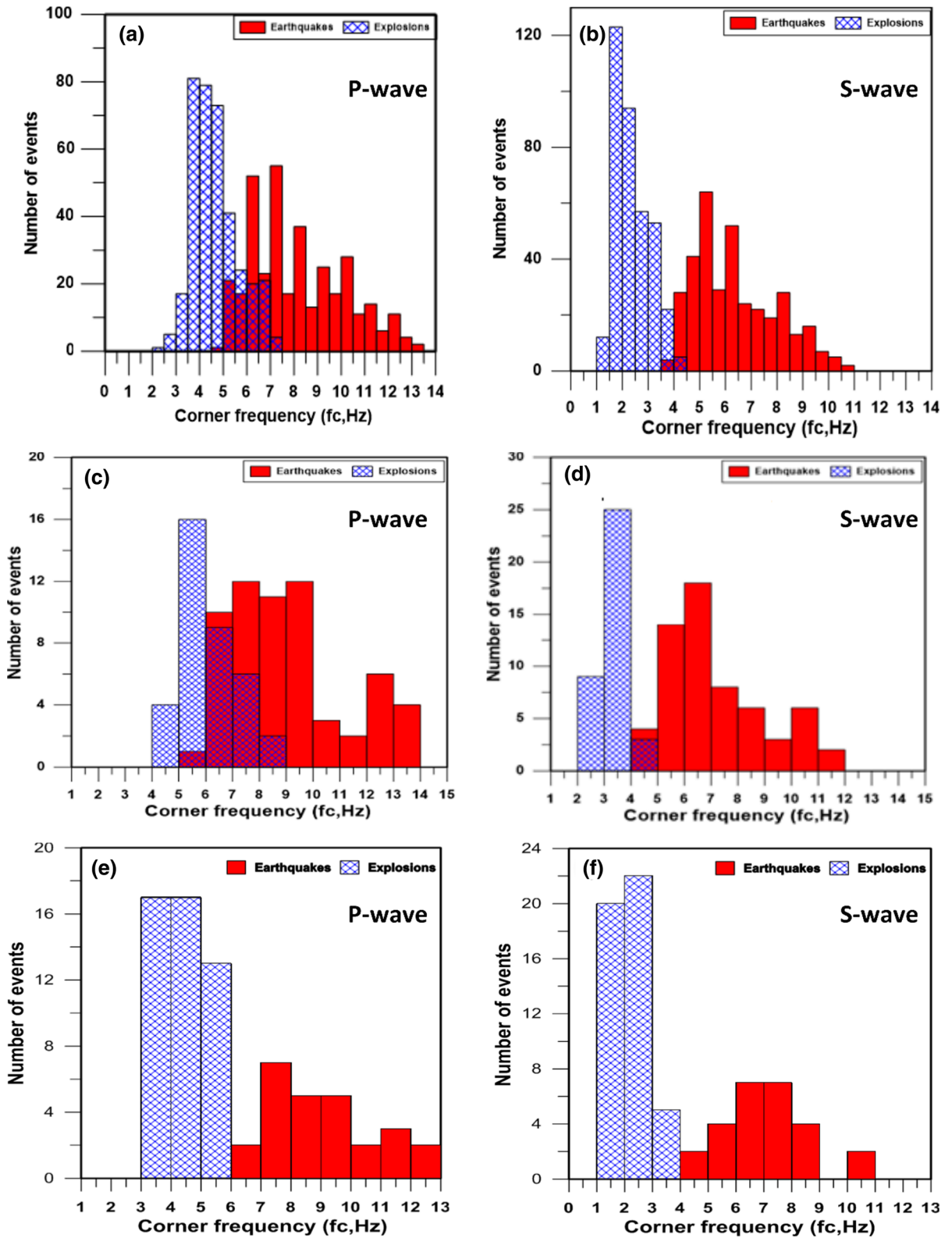
◀Figure 11
Histograms showing distributions of the corner frequency for studied earthquake (red) and explosions (blue cross) in Northern, Central and Southern Egypt obtained from P-wave (**a**, **c**, **e**) and S-wave spectra (**b**, **d**, **f**)

and explosions for P- and S-waves in Northern, Central and Southern Egypt, respectively.

3.2.2 Corner Frequency of P-Waves Vs. Corner Frequency of S-Waves

Ataeva et al. (2017) showed that the average ratio $f_c(P)/f_c(S)$ is higher for explosions than earthquakes. This has highlighted the ability to use this approach as a discriminating method. Figure 12 compares the corner frequencies of P- and S-waves from earthquakes and explosions in Northern, Central and Southern Egypt, respectively. This figure shows a

significant clear separation between earthquakes and explosions. Moreover, earthquakes generally have a smaller $f_c(P)$ shift relative to $f_c(S)$, while explosions show a larger one. The obtained average $f_c(P)/f_c(S)$ ratio is 1.28, 1.26 and 1.26 for earthquakes with a standard deviation of 0.41, 0.63 and 0.52 and a determination coefficient of 0.99, 0.98 and 0.99 for Northern, Central and Southern Egypt, respectively. For explosions, $f_c(P)/f_c(S)$ is 1.89, 1.86 and 2.0 with a standard deviation of 0.34, 0.29 and 0.44 and a determination coefficient of 0.98, 0.99 and 0.97 within the three regions, respectively (Table 4). Based on our findings presented in Fig. 12, the average $f_c(P)$ is larger than the average $f_c(S)$ for both events, but the average ratio $f_c(P)/f_c(S)$ is larger for explosions. Therefore, this result proved the ability of using $f_c(P)/f_c(S)$ ratio as a discriminant tool between earthquakes and explosions. A relation between $f_c(P)/f_c(S)$ ratio and moment magnitude M_w estimated from P- and S-waves are constructed for all three regions

Table 3

Values of corner frequencies f_c (Hz) of the studied earthquakes and explosions in Northern, Central and Southern Egypt for P- and S-waves, separately

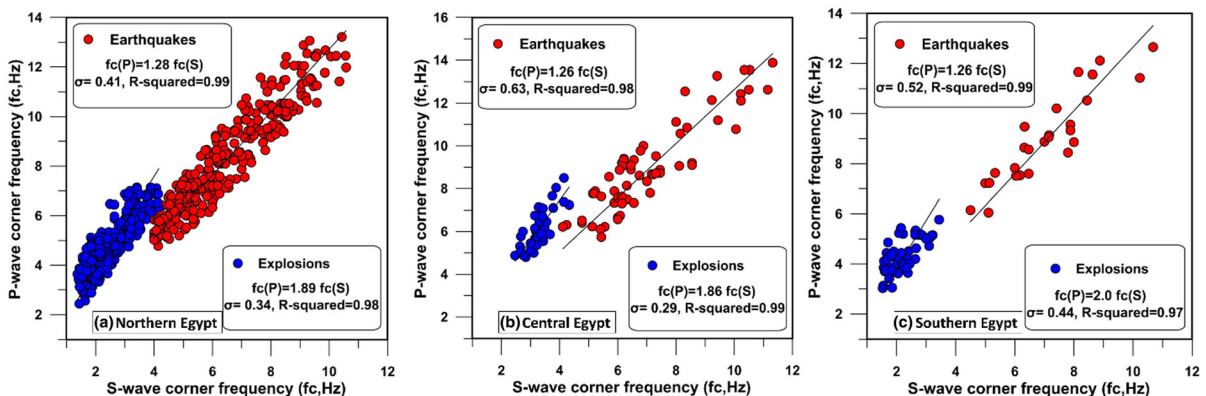| Events	Northern Egypt		Central Egypt		Southern Egypt	
	P-wave	S-wave	P-wave	S-wave	P-wave	S-wave
Earthquakes	4.78–13.21	4–13.21	5.8–14	4.8–12.0	6–13	4.9–11
Explosions	2.44–7.14	1.37–4.16	4.7–9.0	2.8–4.8	3–5.9	1.8–3.9

Figure 12
P-wave corner frequency f_c (P) vs. S-wave corner frequency f_c (S) for earthquakes (red) and explosions (blue) in Northern, Central and Southern Egypt. The black solid lines indicate the least square linear fitting to the data. The estimated values of standard deviation σ and coefficient of determination (R^2) are also shown

Table 4

Obtained average $f_c(P)/f_c(S)$ ratios with their standard deviations σ and determination coefficient R^2 for studied earthquakes and explosions in Northern, Central and Southern Egypt

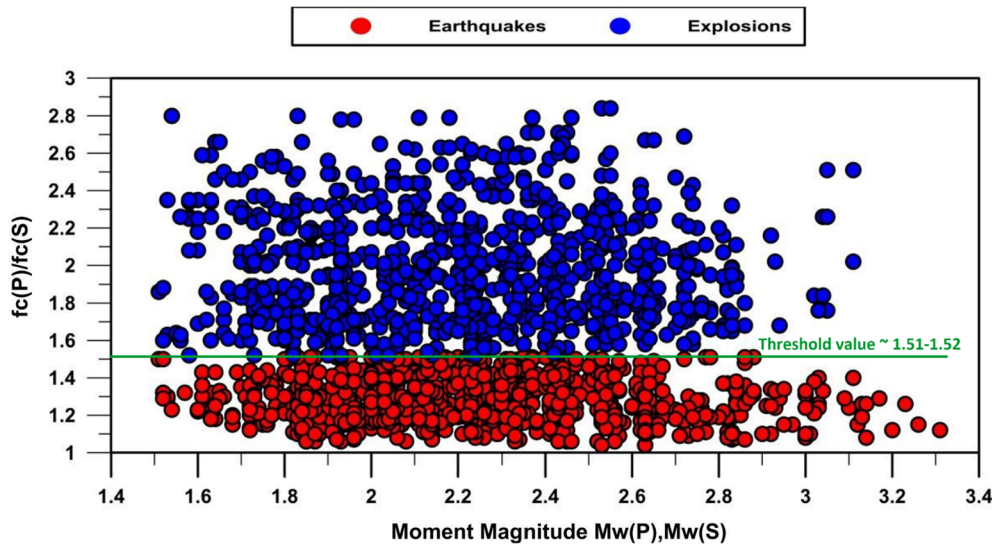| Events	Northern Egypt	Central Egypt	Southern Egypt
Earthquakes	1.28	1.26	1.26
	$\sigma = 0.41$, $R^2 = 0.99$	$\sigma = 0.63$, $R^2 = 0.98$	$\sigma = 0.52$, $R^2 = 0.99$
Explosions	1.89	1.86	2.0
	$\sigma = 0.34$, $R^2 = 0.98$	$\sigma = 0.29$, $R^2 = 0.99$	$\sigma = 0.44$, $R^2 = 0.97$

Figure 13
Ratio between the corner frequencies $f_c(P)/f_c(S)$ from P- and S-waves vs. moment magnitude M_w for earthquakes (red) and explosions (blue) in the three Egyptian regions. The green line represents the empirical discrimination threshold value ∼ 1.51–1.52 for Egypt

in Egypt (Fig. 13). The ratios $f_c(P)/f_c(S)$ are independent of estimated moment magnitude M_w and range from 1.04 to 1.51 (average 1.28) for earthquakes, while explosions display a range between 1.52 and 2.84 (average 1.97). The $f_c(P)/f_c(S)$ discrimination threshold value for segregating of quarry explosions from earthquakes in Egypt is estimated to be around ∼ 1.51–1.52 (Fig. 13). The empirical threshold value is derived by averaging the highest earthquake ratio $f_c(P)/f_c(S)$ and the lowest explosion ratio $f_c(P)/f_c(S)$. Furthermore, the analysis shows a broad dispersion in the corner frequency ratios of explosions.

4. Discussion and Conclusions

In this study, the spectral analysis technique is used to differentiate between earthquakes and quarry blasts in three regions (Northern, Central and Southern) Egypt. The most common approach in spectral analysis is to analyze and compare the corrected P- and S-waves displacement spectra for earthquakes and explosions with comparable magnitudes in each Egyptian region. This study manifested a significant difference between earthquakes and explosions in their spectral properties, focusing on the displacement spectra corner frequency that provided better information about the type of seismic source.

The waveform data processing involved instrumental correction, windowing of selected P and S waves of time histories, integration, calculating the displacement Fourier spectrum and correcting the path effect. Two principal spectral parameters are then extracted from the corrected spectra: the low-frequency spectral level Ω_0 and the corner frequency f_c. Based on Brune's source model, these two parameters are identified using nonlinear least square inversion techniques. The source parameters (f_c, M_o and M_w) are estimated with their standard deviations averaged over several recording stations for the same event. The obtained relatively small values of standard deviations of the average source parameters for earthquakes and explosions suggested that our approach is valid. Then, a quantitative and comparative discrimination analysis was performed for P- and S-waves separately to establish some criteria for distinguishing between earthquakes and explosions in each of the three Egyptian regions.

Our findings showed that the displacement spectra of the quarry blasts demonstrated the lack of high-frequency energy, especially in S-waves. Moreover, we observed a steeper fall off (decrease more sharply with increasing frequency) of the quarry blasts spectra than those of earthquakes spectra that showed a more stable pattern in the three regions. Therefore, the apparent corner frequencies of the P-wave and especially the quarry blasts' S-wave are lower than those for earthquakes of comparable magnitudes. Many researchers also observed similar findings in quarry blast spectra (Bennett & Murphy, 1986; Gitterman, et al., 1998; Shearer & Allmann, 2007; Taylor et al., 1988). In addition, Su et al. (1991), Aki (1995) and Yavuz et al. (2019) also observed that the quarry blast spectra decreased more sharply with increasing frequency than earthquake spectra, leading to a lower corner frequency estimate. Allmann et al. (2008) analyzed and compared the P-wave displacement spectra of different events in Southern California. They obtained a lower corner frequency of quarry blast than earthquake spectra. A steeper fall of the spectra was also observed for quarry blasts.

In this study, our findings showed that the high-frequency P/S spectral amplitude ratio resulting from the difference in corner frequencies for both earthquakes and explosions acted as an effective discriminator between earthquakes and quarry blasts. Ataeva et al. (2017) compared the displacement spectra of the P/S ratio for earthquakes and explosions and obtained the same findings. However, similar findings were also observed for nuclear explosion monitoring; the spectral ratio of regional phases (i.e., Pn/Lg, Pn/Sn, Pg/Lg, Pg/Sn) was an effective discriminant at high frequencies. Many studies have shown that regional spectral amplitude ratios effectively discriminate between earthquakes and nuclear explosions, typically at higher frequencies above about 3 to 4 Hz for test sites in China and northern Russia (e.g., Fisk, 2006; Xie & Patton, 1999). Results obtained from these studies indicated that the spectral amplitude ratios Pn/Lg, Pn/Sn, Pg/Lg and Pg/Sn manifested a good separation between earthquakes and explosions at higher frequencies at all of the hard-rock test sites, which was explained in terms of the difference in the corner frequencies of P phases and Sn- or Lg-waves for nuclear explosions.

For each region in Egypt, we constructed discrimination relations M_o (P,S) vs. f_c (P,S) and f_c (P) vs. f_c (P,S). The first relation manifested that earthquakes and explosions are clearly isolated by the S-wave compared with the P-wave, and the calculated corner frequencies of explosions are lower than those of earthquakes for both types of waves. As a result, M_o vs. f_c can be used as a discriminant graph, depending on the corner frequency. Furthermore, comparing the three Egyptian regions, the Southern region gives a strong and clear separation of corner frequency values of earthquakes and explosions for both waves, in contrast to the other two regions, which showed a slight interference in the corner frequency distributions. However, the variation in M_o vs. f_c among the three Egyptian regions could be attributed to various near-surface geologies, particularly in explosion-prone areas. The near-source (explosion) geological properties caused a change in the spectral characteristics (spectral slope and corner frequency) (Ford et al., 2011; Walter et al., 1995). The different blasting techniques and practices used in the various regions, including delay in ripple-firing (delay time) and blast hole arrangement, also caused changes in the spectral characteristics, particularly the corner frequency.

In the study, our results demonstrated that, for both earthquake and explosion regions, the average $f_c(P)$ is essentially larger than $f_c(S)$. This result was in agreement with previous studies (Hanks & Wyss, 1972; Molnar et al., 1973; Tusa & Gresta, 2008; Watanabe et al., 1996). It is also noted that the average ratio between $f_c(P)$ and $f_c(S)$ is larger for explosions than for earthquakes. This means that the $f_c(P)$ vs. $f_c(S)$ relationship can be used to discriminate between earthquakes and explosions. Based on the $f_c(P)$ vs. $f_c(S)$ discriminant, we also observed a substantial clear separation between earthquakes and explosions in all three regions. In this study, the average empirical ratio $f_c(P)/f_c(S)$ for earthquakes ranges from 1.26 to 1.28 in the various Egyptian regions. This ratio is slightly higher than the values estimated by Ataev et al. (2015, 2017) in Israel and Lebanon. This is most likely because of regional differences in geological conditions and material properties of the propagation medium of each region, which will influence signal amplitude characteristics. In this study, the $f_c(P)/f_c(S)$ ratio for explosions ranges from 1.86 to 2.0 in the various Egyptian regions. The ratio computed by Ataeva et al. (2017) matches those of the Northern Egyptian region, while the other two regions yield slightly higher ratios. The $f_c(P)/f_c(S)$ ratio is considered an effective discriminant for separating earthquakes and explosions in Egypt as it is unaffected by the moment magnitude M_w. The obtained $f_c(P)/f_c(S)$ discrimination threshold value for distinguishing quarry explosions from earthquakes in Egypt is 1.51–1.52. This value represents the separating line between the average maximum value of $f_c(P)/f_c(S)$ for earthquakes and the average minimum value of explosions. The significant scatter in the explosion corner frequency ratios was attributed to the disparity in the ripple fire delay and the local geology of the nearest source in addition to the potential ambiguity of corner frequency estimation.

Declarations

Publisher's Note Springer Nature remains neutral with regard to jurisdictional claims in published maps and institutional affiliations.

References

Abercrombie, R., & Leary, P. (1993). Source parameters of small earthquakes recorded at 2.5 km depth, Cajon Pass, southern California: Implications for earthquake scaling. *Geophysical Research Letters, 20*(14), 1511–1514.

Abou Elenean, K. A., Mohamed, A. M., & Hussein, H. M. (2010). Source parameters and ground motion of the Suez-Cairo shear zone earthquakes, Eastern Desert, Egypt. *Natural Hazards, 52*(2), 431–451.

Aki, K. (1995). *Discriminating underground explosions from earthquakes using seismic coda waves*. University of Southern California Los Angeles Center for Earth Sciences.

Allmann, B. P., Shearer, P. M., & Hauksson, E. (2008). Spectral discrimination between quarry blasts and earthquakes in southern California. *Bulletin of the Seismological Society of America, 98*(4), 2073–2079.

Anderson, D. L., Ben-Menahem, A., & Archambeau, C. B. (1965). Attenuation of seismic energy in the upper mantle. *Journal of Geophysical Research, 70*(6), 1441–1448.

Anderson, D. N., Walter, W. R., Fagan, D. K., Mercier, T. M., & Taylor, S. R. (2009). Regional multistation discriminants: Magnitude, distance, and amplitude corrections, and sources of error. *Bulletin of the Seismological Society of America, 99*(2A), 794–808.

Archuleta, R. J., Cranswick, E., Mueller, C., & Spudich, P. (1982). Source parameters of the 1980 Mammoth Lakes, California, earthquake sequence. *Journal of Geophysical Research: Solid Earth, 87*(B6), 4595–4607.

Ataev, G., Shapira, A., & Hofstetter, A. (2015). Determination of source parameters for local and regional earthquakes in Israel. *Journal of Seismology, 19*(2), 389–401. https://doi.org/10.1007/s10950-014-9472-x

Ataeva, G., Gitterman, Y., & Shapira, A. (2017). The ratio between corner frequencies of source spectra of P- and S-waves—A new discriminant between earthquakes and quarry blasts. *Journal of Seismology, 21*(1), 209–220.

Barton, N. (2007). *Rock quality, seismic velocity, attenuation and anisotropy* (p. 729). Taylor & Francis Group.

Baumbach, M., & Borman, P. (2012). *Determination of source parameters from seismic spectra. New Manual of Seismological Observatory practice 2 (NMSOP-2)* (pp. 1–7). Deutsches Geo Forschugs Zentrum GFZ.

Bennett, T. J., & Murphy, J. R. (1986). Analysis of seismic discrimination capabilities using regional data from western United States events. *Bulletin of the Seismological Society of America, 76*(4), 1069–1086.

Boore, D. M., & Boatwright, J. (1984). Average body-wave radiation coefficients. *Bulletin of the Seismological Society of America, 74*(5), 1615–1621.

Brune, J. N. (1970). Tectonic stress and the spectra of seismic shear waves from earthquakes. *Journal of Geophysical Research, 75*(26), 4997–5009.

Brune, J. N. (1971). Correction to tectonic stress and the spectra of seismic shear waves from earthquakes. *Journal of Geophysical Research, 76*(20), 5002.

Dahy, S. A., & Hassib, G. H. (2010). Spectral discrimination between quarry blasts and microearthquakes in southern Egypt. *Research Journal of Earth Sciences, 2*, 1–7.

EI-Hadidy, S. (1995). Crustal structure and its related causative tectonics in northern Egypt are using geophysical data. Ph.D. thesis, Ain Shams University.

El-Hadidy, S., Mohamed Adel, M. E., Deif, A., Abu El-Ata, S. A., & Moustafa Sayed, S. R. (2006). Estimation of frequency-dependent coda wave attenuation structure at the vicinity of Cairo Metropolitan area. *Acta Geodaetica Et Geophysica Hungarica, 41*(2), 227–235.

Fisk, M. D. (2006). Source spectral modeling of regional P/S discriminants at nuclear test sites in China and the former Soviet Union. *Bulletin of the Seismological Society of America, 96*(6), 2348–2367.

Ford, S. R., Walter, W. R., Ruppert, S. D., Matzel, E. M., Hauk, T. F., & Gok, R. (2011). *Toward an empirically-based parametric explosion spectral model*. Lawrence Livermore National Lab.

Gitterman, Y., Pinsky, V., & Shapira, A. (1998). Spectral classification methods in monitoring small local events by the Israel seismic network. *Journal of Seismology, 2*(3), 237–256.

Hammer, C., Ohrnberger, M., & Fäh, D. (2013). Classifying seismic waveforms from scratch: A case study in the alpine environment. *Geophysical Journal International, 192*(1), 425–439.

Hanks, T. C., & Kanamori, H. (1979). A moment magnitude scale. *Journal of Geophysical Research: Solid Earth, 84*(B5), 2348–2350.

Hanks, T. C., & Wyss, M. (1972). The use of body-wave spectra in the determination of seismic-source parameters. *Bulletin of the Seismological Society of America, 62*(2), 561–589.

Havskov, J., & Ottemöller, L. (2010). Array processing. *Routine data processing in earthquake seismology* (pp. 283–297). Springer.

Horasan, G., Güney, A. B., Küsmezer, A., Bekler, F., Öğütçü, Z., & Musaoğlu, N. (2009). Contamination of seismicity catalogs by quarry blasts: An example from Istanbul and its vicinity, northwestern Turkey. *Journal of Asian Earth Sciences, 34*(1), 90–99.

Kiratzi, A., & Louvari, E. (2001). Source parameters of the Izmit-Bolu 1999 (Turkey) earthquake sequences from teleseismic data. *Annals of Geophysics, 44*(1), 33–47.

Koch, K., & Fäh, D. (2002). Identification of earthquakes and explosions using amplitude ratios: The Vogtland area revisited. *Monitoring the comprehensive nuclear-test-ban treaty: Seismic event discrimination and identification* (pp. 735–757). Birkhäuser.

Kumar, A., Kumar, A., Mittal, H., Kumar, A., & Bhardwaj, R. (2012). Software to estimate earthquake spectral and source parameters. *International Journal of Geosciences, 3*(5), 1142–1149.

Kumar, A., Kumar, R., & Ghangas, V. (2014). Matlab codes to estimate signal to noise ratios (SNR) for P, S and Coda waves.

McLaughlin, K. L., Bonner, J. L., & Barker, T. (2004). Seismic source mechanisms for quarry blasts: Modelling observed Rayleigh and Love wave radiation patterns from a Texas quarry. *Geophysical Journal International, 156*(1), 79–93.

Molnar, P., Tucker, B. E., & Brune, J. N. (1973). Corner frequencies of P and S waves and models of earthquake sources. *Bulletin of the Seismological Society of America, 63*(6–1), 2091–2104.

Motlagh, S. A., & Mostafazadeh, M. (2008). Source parameters of the Mw 5.8 fin (South of Iran) earthquake of March 25, 2006. *World Applied Sciences Journal, 4*(1), 104–115.

Mukhopadhyay, S., Singh, B., & Mohamed, H. (2016). Estimation of attenuation characteristics of Aswan reservoir region, Egypt. *Journal of Seismology, 20*(1), 79–92.

Sertçelik, F., Yavuz, E., Birdem, M., & Merter, G. (2020). Discrimination of the natural and artificial quakes in the Eastern Marmara Region, Turkey. *Acta Geodaetica Et Geophysica, 55*(4), 645–665.

Shearer, P. M., & Allmann, B. P. (2007). Spectral studies of shallow earthquakes and explosions in Southern California. In *Proceedings of the 29th Monitoring Research Review: Ground-Based Nuclear Explosion Monitoring Technologies*, 656–662.

Singh, S. K., Apsel, R. J., Fried, J., & Brune, J. N. (1982). Spectral attenuation of SH waves along the Imperial fault. *Bulletin of the Seismological Society of America, 72*(6A), 2003–2016.

Snoke, A. (2003). Focal mechanism determination software (FOCMEC package). (International Geophysics). In *International Handbook of Earthquake and Engineering Seismology*, 1629–1630. https://doi.org/10.1016/s0074-6142(03)80291-7

Su, F., Aki, K., & Biswas, N. N. (1991). Discriminating quarry blasts from earthquakes using coda waves. *Bulletin of the Seismological Society of America, 81*(1), 162–178.

Süle, B., & Wébe, Z. (2013). Earthquake source parameters and scaling relationships in Hungary (central Pannonian basin). *Journal of Seismology, 17*(2), 507–521.

Taylor, S. R., Sherman, N. W., & Denny, M. D. (1988). Spectral discrimination between NTS explosions and western United States earthquakes at regional distances. *Bulletin of the Seismological Society of America, 78*(4), 1563–1579.

Tusa, G., & Gresta, S. (2008). Frequency-dependent attenuation of P waves and estimation of earthquake source parameters in southeastern Sicily, Italy. *Bulletin of the Seismological Society of America, 98*(6), 2772–2794.

Walter, W. R., Mayeda, K. M., & Patton, H. J. (1995). Phase and spectral ratio discrimination between NTS earthquakes and explosions. Part I: Empirical observations. *Bulletin of the Seismological Society of America, 85*(4), 1050–1067.

Watanabe, K., Sato, H., Kinoshita, S., & Ohtake, M. (1996). Source characteristics of small to moderate earthquakes in the Kanto region, Japan: Application of a new definition of the S-wave time window length. *Bulletin of the Seismological Society of America, 86*(5), 1284–1291.

Xie, J., & Patton, H. J. (1999). Regional phase excitation and propagation in the Lop Nor region of central Asia and implications for P/Lg discriminants. *Journal of Geophysical Research: Solid Earth, 104*(B1), 941–954.

Yavuz, E., Sertçelik, F., Livaoğlu, H., Woith, H., & Lühr, B. G. (2019). Discrimination of quarry blasts from tectonic events in the Armutlu Peninsula, Turkey. *Journal of Seismology, 23*(1), 59–76.

Yilmaz, Ş, Bayrak, Y., & Çınar, H. (2013). Discrimination of earthquakes and quarry blasts in the eastern Black Sea region of Turkey. *Journal of Seismology, 17*(2), 721–734.